Interfacial Coordination Assembly of Tannic Acid with Metal ions on Three-Dimensional Nickel Hydroxide Nanowalls for Efficient Water Splitting

Yueqing Wang,[a, b] Si Chen,[a] Shuya Zhao,[a] Qianwu Chen[a] and Jintao Zhang* [a, b]

1. Key Laboratory for Colloid and Interface Chemistry of State Education Ministry, School of Chemistry and Chemical Engineering, Shandong University, Jinan 250100 (China).
2. Shenzhen Research Institute of Shandong University, Virtural University Park, Nanshan, Shenzhen 518057, Guangdong, China

E-mail: jtzhang@sdu.edu.cn

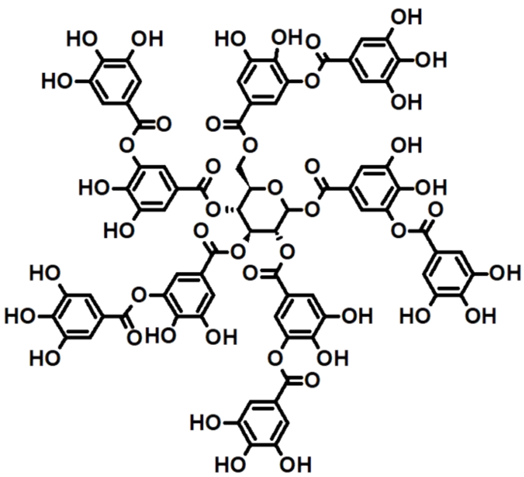

Fig. S1. Molecular structure of tannic acid.

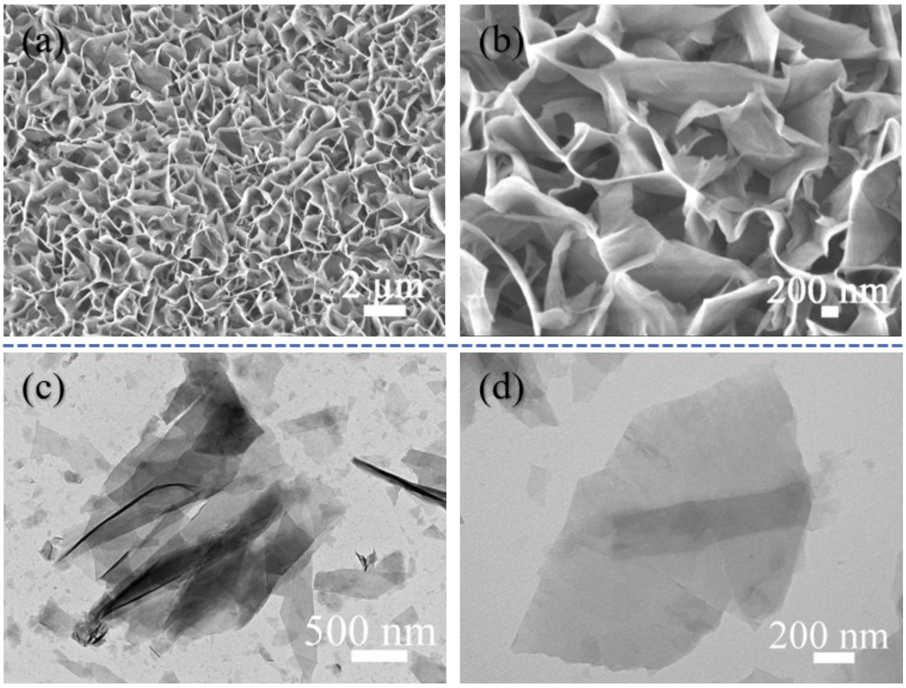

Fig. S2. (a, b) SEM images and (c, d) TEM images of $Ni(OH)_2$ nanosheet array.

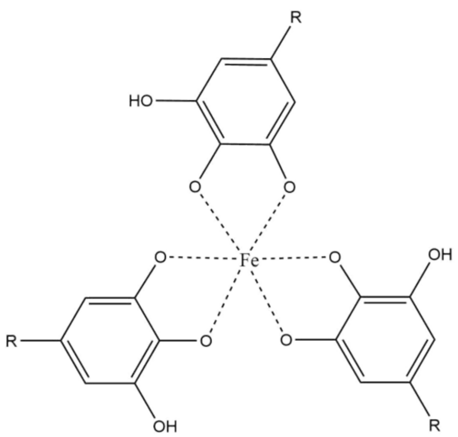

Fig. S3. The dominant complexation state of TA-Fe at pH > 7.

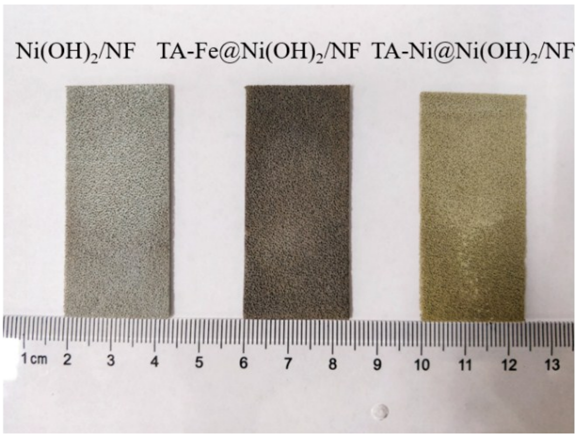

Fig. S4. Digital photo of $Ni(OH)_2$/NF, TA-Fe@$Ni(OH)_2$/NF and TA-Ni@$Ni(OH)_2$/NF electrodes.

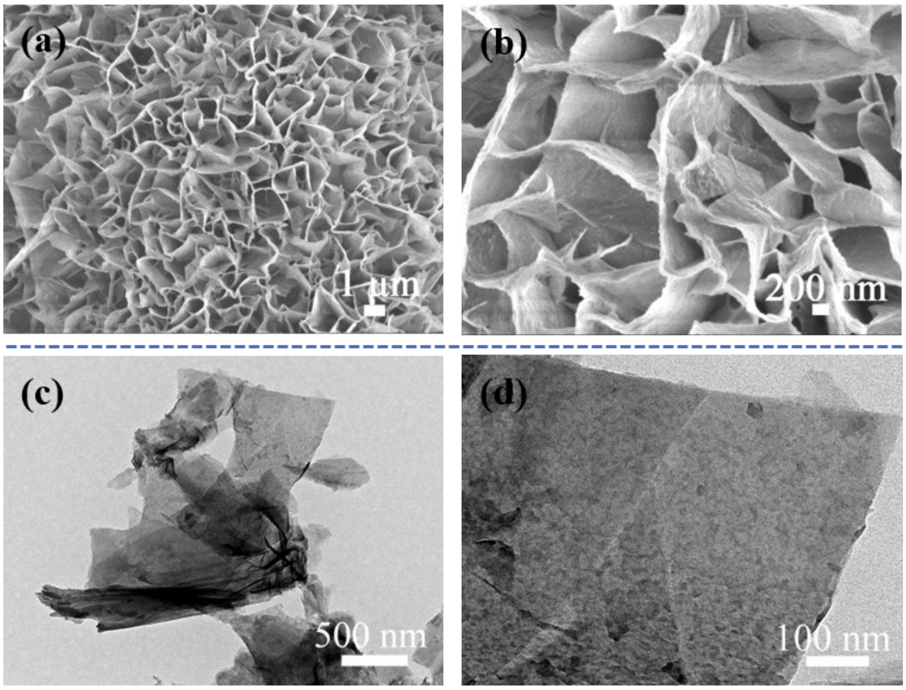

Fig. S5. (a, b) SEM and (c, d) TEM images of TA-Fe@$Ni(OH)_2$/NF.

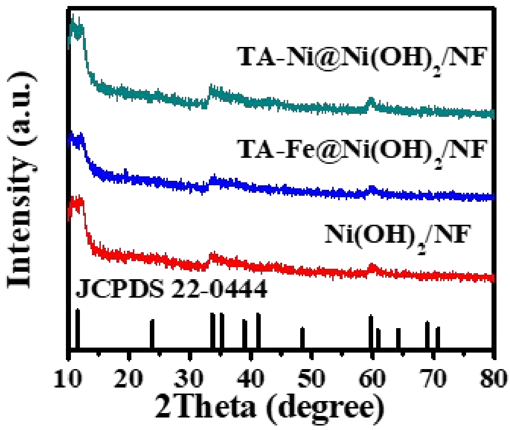

Fig. S6. XRD patterns.

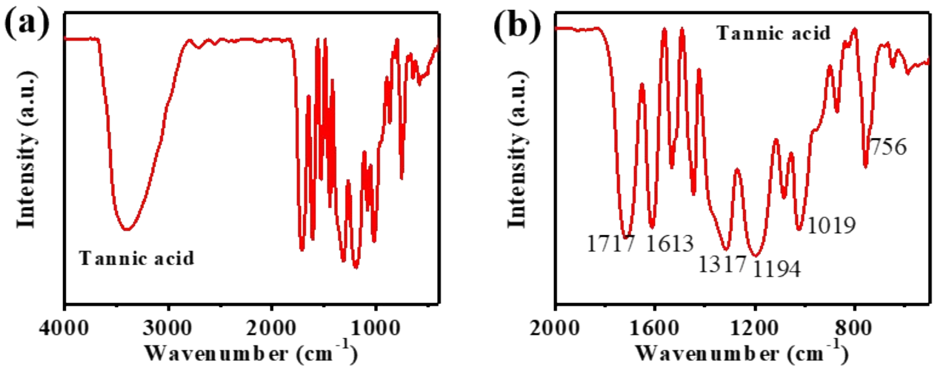

Fig. S7. FTIR spectra of tannic acid.

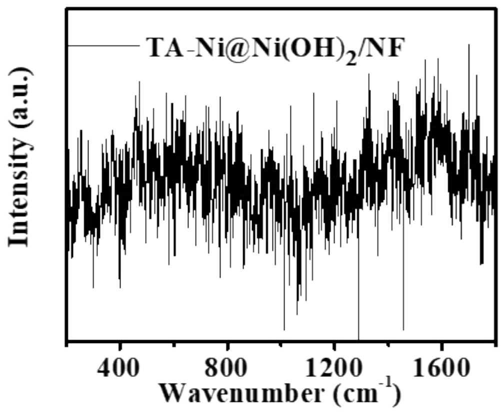

Fig. S8. Raman spectrum of TA-Ni@Ni$(OH)_2$/NF.

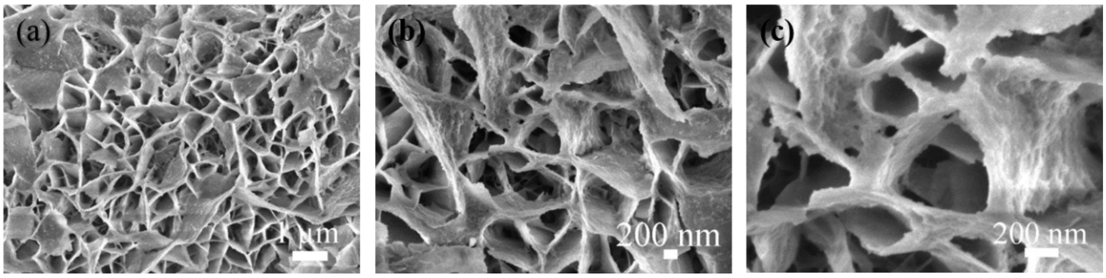

Fig. S9. SEM images of TA-Ni@$Ni(OH)_2$/NF.

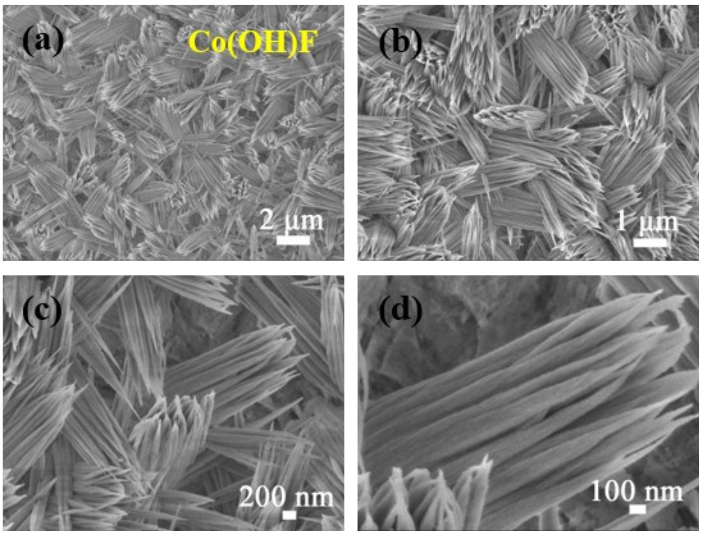

Fig. S10. SEM images of CoOHF nanowires on nickel foam.

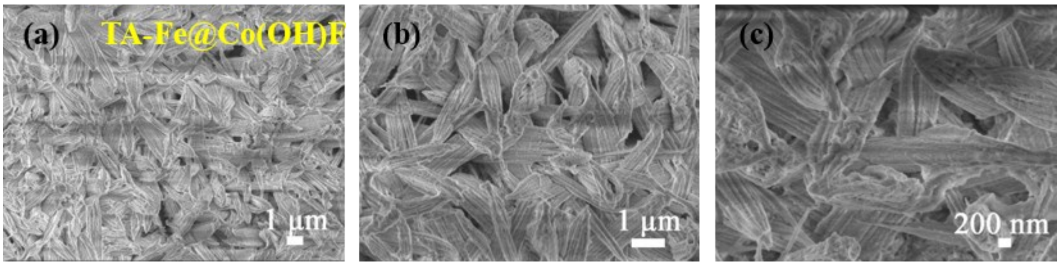

Fig. S11. SEM images of TA-Fe@Co(OH)F hybrid structure.

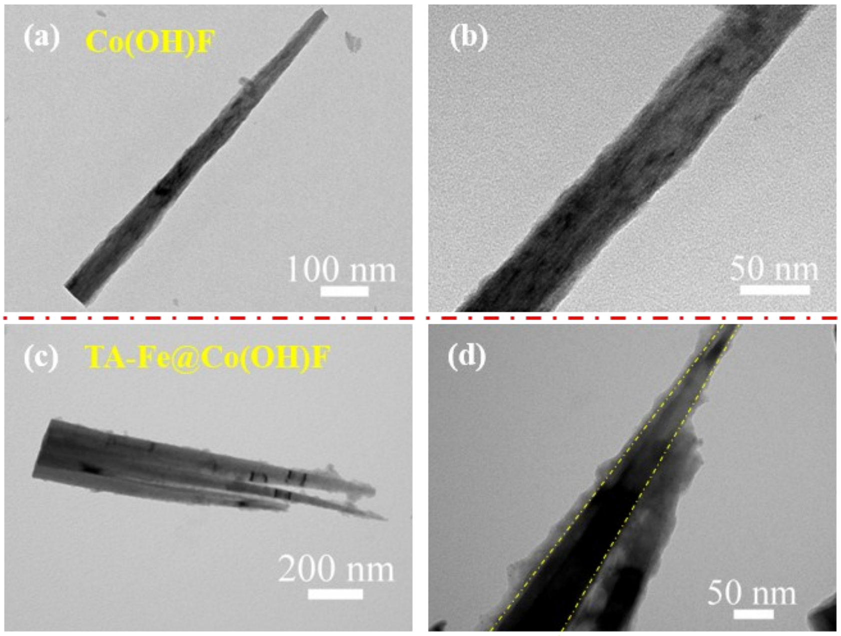

Fig. S12. TEM images of (a, b) Co(OH)F nanowire and (c, d) TA-Fe complex decorated Co(OH)F nanowires.

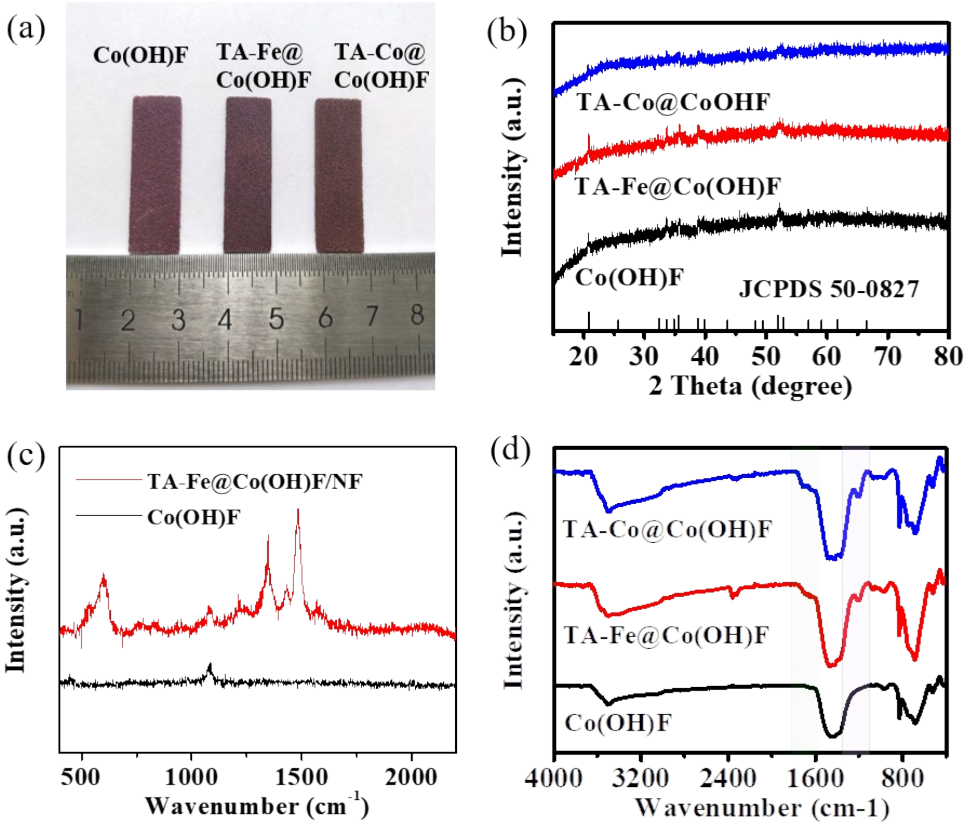

Fig. S13 (a) Digital photo of Co(OH)F/NF, TA-Fe@Co(OH)F/NF and TA-Co@Co(OH)F/NF. (b) XRD patterns. (c) Raman spectra and (d) FTIR spectra.

Co(OH)F nanoarrays on nickel foam were synthesized via hydrothermal method and served as the supporting matrix. With the formation of TA-metal complex layer, the color of Co(OH)F electrode changes obviously from purple to slight brown color (Fig. S13a). However, no obvious XRD diffraction peak of TA-metal is observed for the hybrid electrode (Fig. S13b), suggesting the amorphous nature. In the Raman spectra (Fig. S13c), the obvious peaks located at 535 and 599 cm^{-1} are ascribed to the bidentate complex of TA with Fe^{3+} ions. In addition, the additional peaks at 1711 and 1204 cm^{-1} would also be ascribed to the complex layer (Fig. S13d).

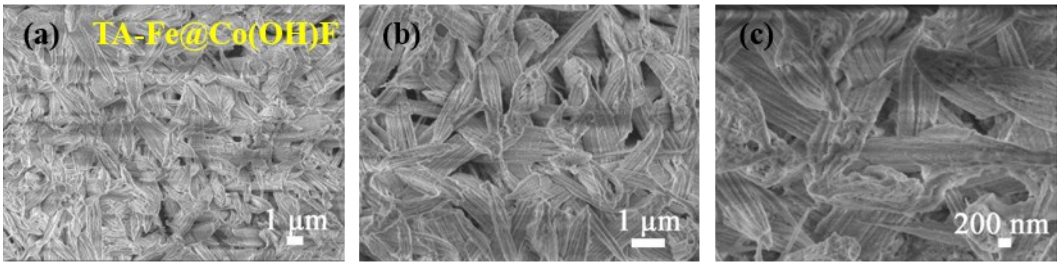

Fig. S14. SEM images of TA-Co@Co(OH)F/NF.

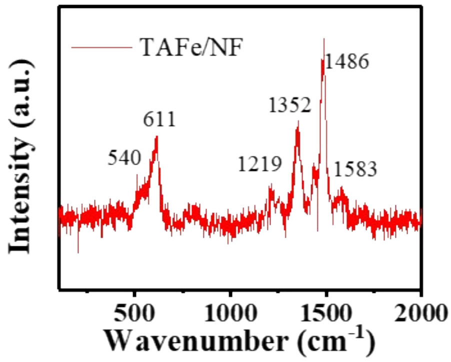

Fig. S15. Raman spectrum of TA-Fe/NF.

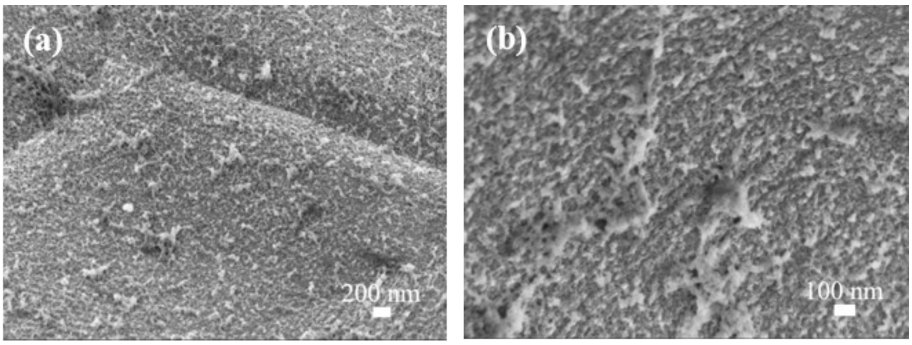

Fig. S16. SEM images of TA-Fe coating on nickel foam.

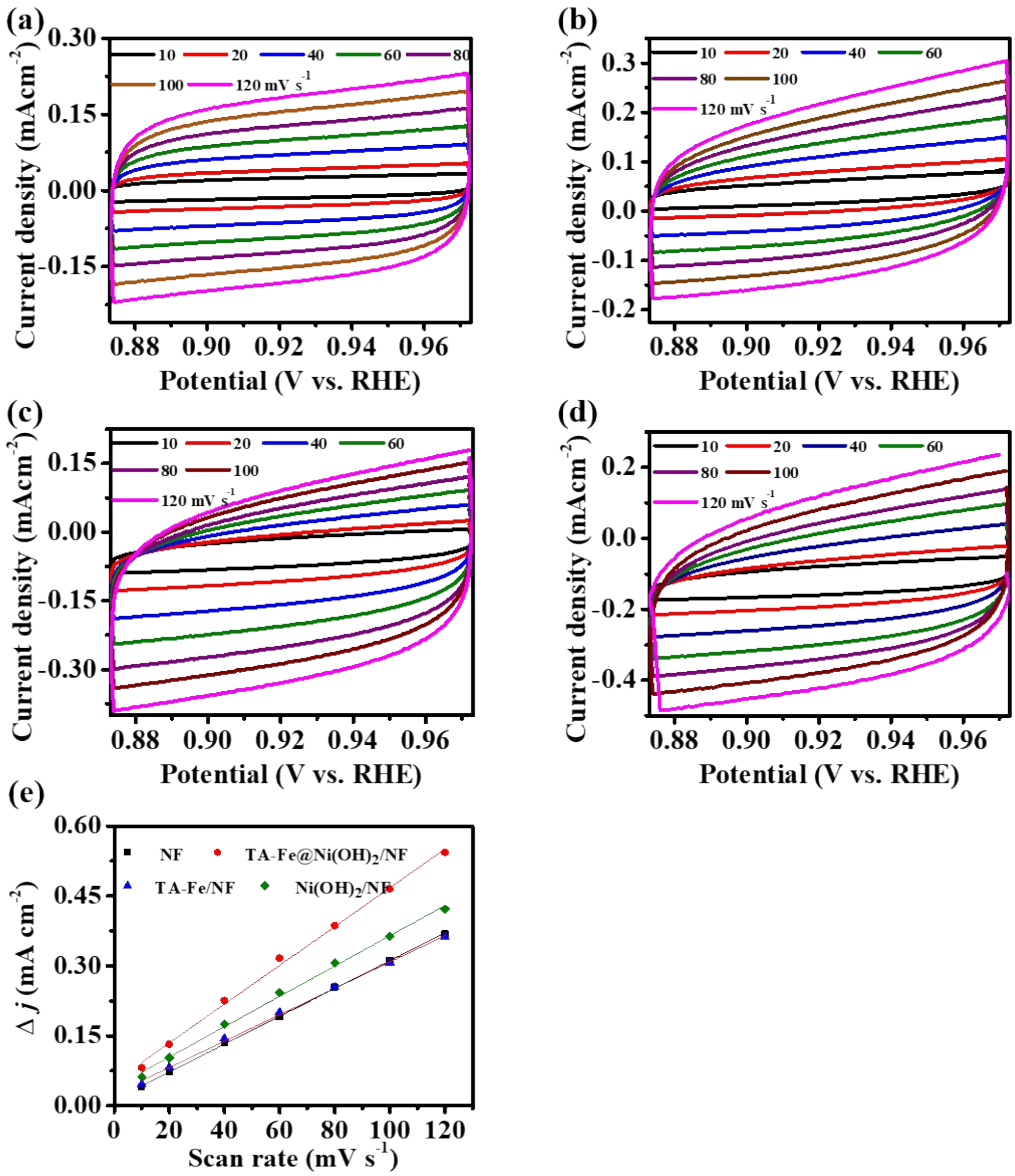

Fig. S17. The CV curves of different electrocatalysts at the scan rates from 10 mV s^{-1} to 120 mV s^{-1}: (a) NF, (b) TA-Fe/NF, (c) $Ni(OH)_2$/NF, (d) TA-Fe@$Ni(OH)_2$/NF. (e) The linear plots of current density changes versus scan rates.

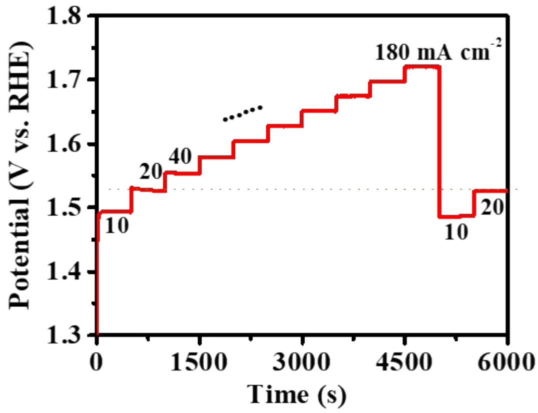

Fig. S18. Multi-step chronoamperometric curves of TA-Fe@Ni$(OH)_2$/NF electrode at different current densities from 10 to 180 mA cm^{-2} and an increment of 20 mA cm^{-2} per 500 s, then back to 20 mA cm^{-2}.

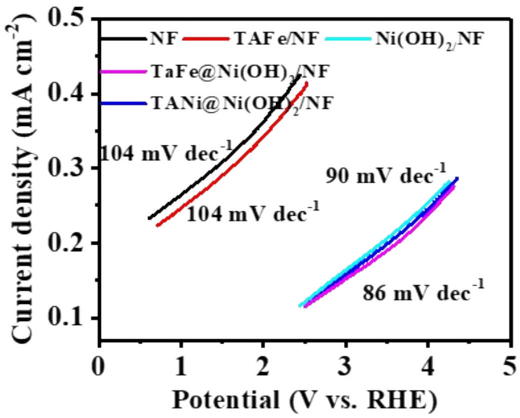

Fig. S19. Tafel plots at various electrodes.

Table S1. The OER performance comparison of different catalyst

Electroatalyst	Electrolyte	Overpotential	Ref.
TA-Fe@Ni(OH)$_2$/NF	1 M KOH	280 mV at 100 mA cm^{-2}	This work
TA-Fe@Ni(OH)$_2$/NF	1 M KOH	306 mV at 350 mA cm^{-2}	This work
TA-Ni@Ni(OH)$_2$/NF	1 M KOH	373 mV at 100 mA cm^{-2}	This work
Ni(OH)$_2$/NF	1 M KOH	380 mV at 100 mA cm^{-2}	This work
TA-Fe/NF	1 M KOH	340 mV at 100 mA cm^{-2}	This work
Ni_3Se_2/NF	1 M KOH	315 mV at 100 mA cm^{-2}	[1]
Ni−Co hydroxide/$Ni_2P_2O_7$	1 M KOH	357 mV at 100 mA cm^{-2}	[2]
CuFe Oxide/CF	1 M KOH	294 mV at 10 mA cm^{-2}	[3]
nPBA@Co(OH)$_2$/NF	1 M KOH	270 mV at 20 mA cm^{-2}	[4]
Ni–S/MIL-53(Fe)/NF	1 M KOH	298 mV at 100 mA cm^{-2}	[5]
NFN-MOF/NF	1 M KOH	335mV at 250 mA cm^{-2}	[6]
BA-NiFe-LDHs/CP	1 M KOH	293 mV at 100 mA cm^{-2}	[7]
V-Ni_3S_2@NiFe LDH/NF	1 M KOH	286 mV at 100 mA cm^{-2}	[8]
FeNiOH/NF	1 M KOH	318 mV at 100 mA cm^{-2}	[9]
CoS_2/Ni_3S_2/CoNiOx	1 M KOH	300 mV at 100 mA cm^{-2}	[10]

Reference

1 A. Sivanantham and S. Shanmugam, *Appl. Catal. B Environ*, 2017, **203**, 485-493.

2 N. R. Chodankar, I. V. Bagal, S. W. Ryu, Y. K. Han and D. H. Kim, *ChemCatChem*, 2019, **11**, 4256-4261.

3 Y. Wang, S. Chen and J. Zhang, *Adv. Funct. Mater.*, 2019, **29**, 1904955.

4 Y. Wang, J. Ma, J. Wang, S. Chen, H. Wang and J. Zhang, *Adv. Energy Mater.*, 2019, **9**, 1802939.

5 F. Wu, X. Guo, G. Hao, Y. Hu and W. Jiang, *Nanoscale*, 2019, **11**, 14785-14792.

6 D. S. Raja, X. F. Chuah and S. Y. Lu, *Adv. Energy Mater.*, 2018, **8**, 1801065.

7 Z. Sun, Y. Wang, L. Lin, M. Yuan, H. Jiang, R. Long, S. Ge, C. Nan, H. Li, G. Sun and X. Yang, *Chem. Commun.*, 2019, **55**, 1334-1337.

8 J. Zhou, L. Yu, Q. Zhu, C. Huang and Y. Yu, *J. Mater. Chem. A*, 2019, **7**, 18118-18125.

9 J.-T. Ren, G.-G. Yuan, C.-C. Weng, L. Chen and Z.-Y. Yuan, *Nanoscale*, 2018, **10**, 10620-10628.

10 H. Lee, X. Wu, Q. Ye, X. Wu, X. Wang, Y. Zhao and L. Sun, *Chem. Commun.*, 2019, **55**, 1564-1567.